Clim Dyn (2015) 45:3493–3511
DOI 10.1007/s00382-015-2552-y

Land-sea warming contrast: the role of the horizontal energy transport

Olivier Geoffroy[1] · David Saint-Martin[1] · Aurore Voldoire[1]

Received: 4 December 2014 / Accepted: 2 March 2015 / Published online: 28 March 2015

Abstract In this study we investigate the role of the mechanisms at play in the magnitude of the land-sea warming contrast and its intermodel spread in the fifth coupled models intercomparison project (CMIP5) simulations. In this aim, an energy-balance model (EBM), with one box representing the land area and two other boxes the near-surface and the deep ocean, is developed. In particular, a simple parameterization of the horizontal energy transport (HET) change between these two regions is proposed. The EBM is shown to capture the variation of the land and the ocean temperature responses and of the land-sea warming ratio in different idealized climate change experiments. By using this framework, we first show that the land-sea warming contrast is explained by the asymmetry in the strength of the HET between the land and ocean and not by land-sea differences in radiative feedbacks. Then we use a method of analysis of variance to infer the contributors to the intermodel spread in the land-sea warming ratio of climate models participating to CMIP5. The main contributor is found to be the HET with a contribution of about 70 %. Finally, our results suggest that the asymmetric character of the HET dependency to the land and the ocean temperature responses may be primarily explained by the land-sea differences in surface specific humidity change for a given temperature change.

✉ Olivier Geoffroy
o.geoffroy@unsw.edu.au

David Saint-Martin
david.saint-martin@meteo.fr

Aurore Voldoire
aurore.voldoire@meteo.fr

[1] CNRM/GAME, Météo-France/CNRS, 42 av. G. Coriolis, 31057 Toulouse, France

Keywords Land-sea contrast · Horizontal energy transport · Forcing adjustment · Radiative feedbacks · Intermodel spread · Energy balance model · Climate sensitivity

1 Introduction

In response to increasing concentrations of greenhouse gases, the mean surface air temperature increases with a larger warming over the land than over the ocean. This land-sea warming contrast is a robust feature of modelled climate change (Manabe et al. 1991; Joshi et al. 2013) and is displayed in observations (Sutton et al. 2007; Drost et al. 2012). The land-sea warming ratio ϕ is defined as the ratio of the mean surface air temperature change over the land to the mean surface air temperature change over the ocean. The range of ϕ exhibited by climate models is consistent with observations (Sutton et al. 2007; Drost et al. 2012) but it varies significantly between climate models, from 1.3 to 1.9 in CMIP3 and CMIP5 1 % year^{-1} CO_2 climate change experiments (Sutton et al. 2007; Joshi et al. 2013). Its value is slightly lower in historical simulations due to the aerosol forcing (Joshi et al. 2013). In addition, the land-sea contrast is displayed at most latitudes with larger amplitude in the subtropics and in the northern extratropics (Sutton et al. 2007).

For a given model, ϕ is relatively time-invariant under different CO_2 increase scenarios (Huntingford and Cox 2000; Joshi et al. 2013). The land-sea contrast is not only a feature of transient warming but is also displayed in equilibrium simulations (Manabe et al. 1991). Most climate models exhibit a smaller ϕ at equilibrium (simulated with a mixing-layer ocean model) than in a climate transition (Sutton et al. 2007). These features can be generalized to

most regions of the climate system as shown by pattern scaling studies (e.g. Geoffroy and Saint-Martin 2014). First, a space-time decomposition based on one single pattern can be used to represent the transient warming under climate change, showing that the ratio of the temperature responses of two given regions of the climate system is relatively time-invariant. Second, the equilibrium pattern differs from that in transition due to the effect of deep-ocean heat uptake that slows down the warming, in particular in the North Atlantic and the circumpolar ocean regions (Manabe et al. 1991).

A particularity of the land is its small heat capacity in comparison with that of the ocean, hence contributing to increase the relative warming over land in transient simulations. However, this feature is not the dominant effect since the land-sea ratio is also displayed in equilibrium simulations (Sutton et al. 2007; Joshi et al. 2008). Moreover, the warming over the land and the ocean is not a local response of the local radiative forcing as shown by idealized simulations in which land and ocean surfaces are perturbed separately by increasing the CO_2 concentration and/or by fixing the surface temperature (Forster et al. 2000; Compo and Sardeshmukh 2009; Lambert et al. 2011). Indeed, the horizontal energy transport (hereafter HET) plays an important role in redistributing in space the incoming energy (Forster et al. 2000; Boer and Yu 2003; Joshi et al. 2013). Thus, a warming over the ocean leads to a warming over the land and reversely (Compo and Sardeshmukh 2009; Lambert et al. 2011; Dommenget 2012). Assuming the horizontal energy transport is the dominant mechanism in constraining ϕ near an invariant value, Lambert and Chiang (2007) derive a formula for the HET change. By using this equation in a two-box energy-balance model, Lambert et al. (2011) show that the qualitative behaviour of the predicted HET is consistent with that observed in idealized experiments. However, the sensitivity of each region (land or ocean) to the other is asymmetric: the ocean is less sensitive to a warming over the land than the land is sensitive to a warming over the ocean. This is partly due to the ocean heat uptake in transition but this is also a general feature of the climate system as shown by equilibrium simulations (Dommenget 2012).

Another manifestation of the land-sea contrast is the warming over the land in response to a CO_2 increase in fixed sea surface temperature (SST) experiments. Such experiments are commonly used to determine the radiative forcing associated with a CO_2 increase (Hansen et al. 1997). In these experiments, the radiative imbalance change is not equal to the stratosphere-troposphere adjusted radiative forcing because it includes a contribution of the radiative response associated with the small temperature increase over land (e.g. Sherwood et al. 2014).

The equilibrium land-sea warming contrast originates from differences in the availability of surface moisture over land and oceans (Manabe et al. 1992). Joshi et al. (2008) point out that these differences lead to different atmospheric temperature lapse rate changes over land and ocean. Hence, if the temperature change in the free troposphere is identical over the land and the ocean then the land-sea warming ratio is larger than one. Byrne and O'Gorman (2013a, b) revisit this idea by developing a theory based on the equality of equivalent potential temperature over land and ocean, and apply it to zonal means. This theory is valid only in the tropics (Byrne and O'Gorman 2013b), where the free-tropospheric temperature is relatively horizontally homogeneous (Sobel and Bretherton 2000) and mean lapse rates over land and ocean are moist adiabatic. In the extratropics, the theory of Joshi et al. (2008) is not valid for heterogeneous perturbations because large spatial differences in diabatic heating counteract the smoothing of the troposphere temperature change by atmospheric energy transport (Joshi et al. 2013). In addition, differences in feedbacks, in particular those associated with clouds and humidity, have been suggested to play a important role (Fasullo 2010).

In this study, we analyse the role of the horizontal heat transport and the other mechanisms at play in the land-sea warming contrast, such as radiative feedbacks, by using energy budget considerations. In this aim, the two-layer energy-balance model framework described in Held et al. (2010), Geoffroy et al. (2013a, b) is adapted to the two boxes decomposition in land and ocean regions, already used in previous studies (Huntingford and Cox 2000; Lambert et al. 2011). A main difference with these studies concern the parameterization of the HET change between the land and the ocean. The framework is described in detail in Sect. 2 and is evaluated in Sect. 3 by using CMIP5 coupled ocean atmosphere climate models idealized experiments and additional idealized experiments dedicated to this study performed with CNRM-CM5. In Sect. 4, this framework is used to analyze the role of each mechanism (forcing, radiative feedbacks, ocean thermal inertia and HET) in the amplitude of the land-sea warming ratio and its contribution to the intermodel spread. The formula for the horizontal energy transport is then briefly discussed. A summary and perspectives are presented in the conclusion.

2 Framework and method

2.1 Theoretical framework

We consider the conceptual two-layer energy-balance model in which the first layer is the atmosphere and near-surface ocean, and the second layer represents the deeper ocean. Here, this simple model is extended to a three-box model by splitting the upper layer into land and ocean

Table 1 Summary of definitions of LO-EBM physical parameters and variables

Parameters and variables	Definiton	Unit
$\mathcal{F}_o$	Adjusted radiative forcing over ocean	$\mathrm{W\,m^{-2}}$
$\mathcal{F}_l$	Adjusted radiative forcing over land	$\mathrm{W\,m^{-2}}$
λ_l	Land radiative response ('feedback') parameter	$\mathrm{W\,m^{-2}K^{-1}}$
λ_o	Ocean radiative response ('feedback') parameter	$\mathrm{W\,m^{-2}K^{-1}}$
γ_o	Heat exchange coefficient between the near-surface ocean and the deeper ocean	$\mathrm{W\,m^{-2}K^{-1}}$
C_l	Surfacic heat capacity of the land	$\mathrm{W\,y\,m^{-2}K^{-1}}$
C_o	Surfacic heat capacity of the upper ocean	$\mathrm{W\,y\,m^{-2}K^{-1}}$
C_{do}	Surfacic heat capacity of the deep ocean	$\mathrm{W\,y\,m^{-2}K^{-1}}$
α_o, α_l	Parameters in the horizontal energy transport formula	$\mathrm{W\,m^{-2}K^{-1}}$
f_l	Land fraction	
ΔT_l	Mean surface air temperature change over land	K
ΔT_o	Mean surface air temperature change over ocean	K
ΔT_{do}	Characteristic deep-ocean temperature change	K
ΔA	Change in horizontal energy transport between land and ocean	$\mathrm{W\,m^{-2}}$
H	Deep-ocean heat uptake	$\mathrm{W\,m^{-2}}$
ΔN_l	Radiative imbalance over land ($=\mathcal{F}_l + R_l$)	$\mathrm{W\,m^{-2}}$
ΔN_o	Radiative imbalance over ocean ($=\mathcal{F}_o + R_o$)	$\mathrm{W\,m^{-2}}$

regions. The state of each box is described by a temperature perturbation ΔT_l, ΔT_o and ΔT_{do}, that verify the following system of equations:

$$C_l \frac{d\Delta T_l}{dt} = \mathcal{F}_l + R_l - \frac{1}{f_l}\Delta A, \tag{1}$$

$$C_o \frac{d\Delta T_o}{dt} = \mathcal{F}_o + R_o + \frac{1}{1-f_l}\Delta A - H, \tag{2}$$

$$C_{do} \frac{d\Delta T_{do}}{dt} = H \tag{3}$$

where C, C_o and C_{do} are the effective heat capacities of the land surface, of the upper and of the deep ocean, respectively (see Table 1), $\mathcal{F}_l$ and $\mathcal{F}_o$ are the radiative forcings over land and ocean, respectively, R_l and R_o are the radiative responses over land and over ocean, respectively, f_l is the land fraction, H is the deep-ocean heat uptake and ΔA is the anomalous atmospheric land-to-ocean horizontal energy transport. Whereas all radiative fluxes, heat content changes and H are expressed per unit area of the considered region, ΔA is expressed per unit of the global area. This explains its normalization by the fraction of total area covered by the considered region in Eqs. (1) and (2). This model will be referred to hereafter as LO-EBM (Land-ocean energy balance model).

The energy fluxes are parametrized as a function of the CO_2 concentration and the LO-EBM variables by performing the following assumptions:

1. The radiative perturbation (including the effect of stratospheric and tropospheric adjustments) associated with the CO_2 change in a given region is assumed to be regional and to vary logarithmically with the regional CO_2 concentration. The forcing adjustment depends on the fast response (a few months) of the atmosphere to the CO_2 change. The magnitude of the tropospheric adjustment is driven by changes in clouds and is model dependent (Gregory and Webb 2008; Vial et al. 2014; Geoffroy et al. 2014). Given the difference in structural atmospheric characteristics over the land and the ocean, the amplitude of the forcing adjustment differs according to the region. In each region, it is assumed to be related to the regional concentration via a parameter that is a reference radiative forcing such as the 4xCO_2 adjusted radiative forcing $\mathcal{F}_i^{4\mathrm{xCO_2}}$:

$$\mathcal{F}_i(t) = \frac{\mathcal{F}_i^{4\mathrm{xCO_2}}}{2\ln(2)} \ln\left(\frac{[\mathrm{CO_2}]_i(t)}{[\mathrm{CO_2}]_i(0)}\right), \tag{4}$$

   where the index i refers to either land or ocean.
2. The heat flux exchange H between the upper and the deeper ocean is assumed to be proportional to the difference between the temperature change of each layer with a heat exchange coefficient γ_o:

$$H = \gamma_o(\Delta T_o - \Delta T_{do}). \tag{5}$$

   This equation differs slightly from the global one of Gregory (2000); Held et al. (2010), H being assumed

to scale with $\Delta T_g - \Delta T_{do}$, where ΔT_g is the global-mean surface air temperature.

3. The radiative response over land/upper-ocean is assumed to be a linear function of the temperature response of the given area only (e.g. Boer and Yu 2003; Crook et al. 2011). This assumption does not take into account potential remote radiative feedbacks, i.e. remote influences, that are not associated with energy exchange between the regions. By assuming a linear dependency with the temperature response, the radiative response over land and ocean reads

$$R_i = -\lambda_i \Delta T_i, \tag{6}$$

where λ_l and λ_o are the radiative response parameters for the land and the ocean regions, respectively. The equations of the radiative imbalance over land and ocean that take into account non-linear effects are described in Sect. 2.2.

4. The heat capacity of the land, C_l, is assumed to be negligible. Note however that observations indicate that the heat gain of the continents is non zero (Beltrami et al. 2002).

5. The anomalous atmospheric land-to-ocean horizontal energy transport ΔA is assumed to be linearly dependent on both ocean and land temperature change:

$$\Delta A = \alpha_l \Delta T_l - \alpha_o \Delta T_o. \tag{7}$$

where the index i refers to either land or ocean. This formula is similar to the one Bates (1999, 2007) used to parameterize the energy transport by atmospheric motions between the tropics and the extratropics. It is similar to a diffusive equation (e.g. Huntingford and Cox 2000) but with a different coefficient associated with each temperature change ΔT_i ($\alpha_o = \alpha_l$ in the diffusive case). It can also be viewed as the sum of two forcings, each one associated with the temperature change over one region: the land exerts a forcing over the ocean and the ocean exerts a forcing over the land. These forcings are linear functions of the land temperature response and the ocean temperature response, respectively. For $\alpha_o > \alpha_l$, a land-sea warming ratio greater than one is favored. Indeed, considering a simple case with equal net radiative flux changes at TOA over land and ocean at equilibrium (i.e. $\Delta A = 0$), a diffusive law ($\alpha_o = \alpha_l$) involves equal warming over land and ocean. For $\Delta A = 0$ and $\alpha_o > \alpha_l$, the warming is larger over land than over ocean. The relative role of the HET change and the other mechanisms in the land-sea warming ratio is discussed in more detail in Sect. 4.1.

An analysis of the CMIP5 4xCO_2 experiment shows that ΔA (taken as the radiative imbalance over land, ΔN_l) is not a linear function of $\Delta T_l - \Delta T_o$ (not shown). This invalides the use of a diffusive equation, in agreement with the results of Huntingford and Cox (2000). However, assuming that the HET change follows a diffusive law as a function of the mid-troposphere temperature change (Joshi et al. 2013), the smaller decrease of the lapse rate over land than over ocean (Joshi et al. 2008) involves $\alpha_o > \alpha_l$ in Eq. (7). The different changes in lapse rates over land and ocean is due to limited moisture availability over land (Joshi et al. 2008). Under some assumptions, the mid-troposphere temperature change can be related to the surface moist static energy change (Byrne and O'Gorman 2013a, b). Hence, a diffusive relationship of the HET change as a function of the MSE change over land and ocean may constitute an adequate approximation of Eq. (7). The validity of such a parameterization as a function of MSE changes, and its role in explaining the relative magnitude of α_o and α_l is discussed in more detail in Sect. 4.3.

Finally, the system of equations reads:

$$0 = \mathcal{F}_l - \lambda_l \Delta T_l + \frac{\alpha_o}{f_l} \Delta T_o - \frac{\alpha_l}{f_l} \Delta T_l, \tag{8}$$

$$\begin{aligned} C_o \frac{d\Delta T_o}{dt} =& \mathcal{F}_o - \lambda_o \Delta T_o - \frac{\alpha_o}{1-f_l} \Delta T_o \\ &+ \frac{\alpha_l}{1-f_l} \Delta T_l - \gamma_o (\Delta T_o - \Delta T_{do}), \end{aligned} \tag{9}$$

$$C_{do} \frac{d\Delta T_{do}}{dt} = \gamma_o (\Delta T_o - \Delta T_{do}), \tag{10}$$

with initial conditions $\Delta T_o(0) = 0$ and $\Delta T_{do}(0) = 0$ for a time-integration from preindustrial conditions. In this system, ΔT_o and ΔT_{do} remain two prognostic variables, whereas ΔT_l is now a diagnostic variable (due to the disappearance of C_l) and is related to ΔT_o by the formula

$$\Delta T_l(t) = \frac{\mathcal{F}_l(t)}{\lambda_l + \alpha_l/f_l} + \frac{\alpha_o/f_l}{\lambda_l + \alpha_l/f_l} \Delta T_o(t). \tag{11}$$

From this equation, it directly follows that the surface temperature over land evolves with identical time scales to that of the ocean. Indeed, it is the sum of a term proportional to the ocean warming and a shift proportional to the land forcing amplitude, defined as the land fast-adjustment temperature.

2.2 Land fast-adjustment temperature

The land fast-adjustment temperature ΔT_l^{adj} is the fast temperature response of the land to the external radiative perturbation. This change has a characteristic time scale of a

few months and is therefore considered as being instantaneous. This change is that obtained without any ocean surface air temperature change ($\Delta T_o = 0$ in Eq. 11):

$$\Delta T_l^{adj}(t) = \frac{\mathcal{F}_l(t)}{\lambda_l + \alpha_l/f_l}. \tag{12}$$

The land fast-adjustment temperature ΔT_l^{adj} is a function of the radiative forcing over land, of the response parameter λ_l and is limited by the magnitude of the energy transport from the land to the oceans via its dependency to the parameter α_l. Without any horizontal energy transport ($\alpha_i = 0$), the land fast response would instantaneously adjust to the equilibrium response (because C_l is 0) equal to $\mathcal{F}_l(t)/\lambda_l$ in this case.

In the case of a step forcing, ΔT_l^{adj} is constant in time and represents the value to which ΔT_l instantaneously adjusts. This change corresponds to the temperature response over land obtained in a fixed SST experiment with a CO_2 increase (Hansen et al. 1997). Note that, disregarding limitations associated with the framework, this statement is not rigorously true: despite the SST being fixed in such experiment, the mean surface air temperature over the ocean slightly increases adding to a very small contribution of the second RHS term of Eq. (11). In a 1 % year^{-1} CO_2 experiment, ΔT_l^{adj} increases linearly with time as does the radiative forcing.

2.3 Land-sea warming ratio

Within this conceptual framework, the land-sea warming ratio ϕ reads:

$$\phi(t) = \frac{\alpha_o/f_l}{\lambda_l + \alpha_l/f_l} + \frac{\Delta T_l^{adj}(t)}{\Delta T_o(t)}. \tag{13}$$

ϕ is the sum of two terms: a constant term ϕ' and a term that depends on the ratio of the land fast-adjustment temperature to the ocean temperature response. Hence, in the case of a step forcing, the temporal evolution of ϕ is a linear function of $1/\Delta T_o$. It is infinite at $t = 0$, decreases quickly during the first years and slowly decreases during the remaining few thousand years until equilibrium.

Note that an equivalent formula to Eq. (7) for ΔA can be obtained by combining Eqs. (8) and (11):

$$\frac{\Delta A}{f_l} = \mathcal{F}_l - \lambda_l \Delta T_l^{adj} + \alpha' \Delta T_o \tag{14}$$

where $\alpha' = -\lambda_l \alpha_o/(f_l \lambda_l + \alpha_l)$. For a step forcing, the heat initially transferred from the land to the ocean is the forcing over land $f_l \mathcal{F}_l$ minus the radiative restoring induced by the land fast adjustment. Then ΔA is reduced with the increase of ΔT_o ($\alpha' < 0$). By fixing $\Delta T_l^{adj} = 0$ in Eq. (14), this formula is equivalent to that of Lambert et al. (2011), obtained by imposing ϕ to a constant value. In the LO-EBM, the value of ϕ is not imposed.

2.4 Consideration of non-linear behaviours

Some climate models exhibit a non-linear relationship between (1) the radiative imbalance as a function of the temperature over land or ocean and between (2) $\Delta T_l - \Delta T_l^{adj}$ as a function of ΔT_o (see Sect. 3.1). During a climate transition the warming slows down due to the large ocean thermal inertia (Hansen et al. 1984), in particular in the North Atlantic and the Circumpolar Ocean regions (Manabe et al. 1991). As a result of the different nature of the perturbations involved, CO_2 forcing and ocean heat uptake, and the differences in their associated temperature patterns, the strength of the radiative feedbacks may differ in transition and in equilibrium (Winton et al. 2010; Geoffroy et al. 2013b; Rose et al. 2014). Consistent with this theory, the ocean radiative imbalance evolves non-linearly as a function of the temperature response for some climate models (see Sect. 3 and Fig. 2). For some models, a slight non-linear relationship is also depicted over the land. Indeed, due to its tight coupling with the ocean temperature, the warming may also slow down in some land regions. In particular the temperature homogenizes quickly over latitude (Joshi et al. 2013). Similar to the strength of the radiative response, due to the relationship between the HET and the temperature pattern, α_l and α_o may also vary with the amplitude of the ocean heat uptake.

The non-linearities may be taken into account by introducing an efficacy factor (Hansen et al. 2005) that relates the equilibrium value of the given parameter and its value for an imposed deep-ocean heat-uptake (Winton et al. 2010; Held et al. 2010; Geoffroy et al. 2013b). The system of equations taking into account these non-linearities is given in the Appendix. This system incorporates three additional parameters. Two radiative parameters are introduced to take into account the non-linearity of ΔN_o and ΔN_l against ΔT_o and ΔT_l, respectively. One parameter is introduced to take into account the non-linearity of ΔT_l against ΔT_o. The 9-parameter EBM (presented in Sect. 2.1) and the 13-parameter EBM (presented in the Appendix) are hereafter referred to as the linear LO-EBM and the non-linear LO-EBM, respectively.

2.5 Method for parameter calibration

The method used to determine the value of the parameters of the LO-EBM is adapted from Geoffroy et al. (2013b). In the following, the method presented is that used to calibrate the nine parameters of the linear LO-EBM. The calibration of the EBM version that represents non-linear behaviour is described in the Appendix. The parameters are determined

from the TOA radiative net flux change and the surface temperature change both over land and oceans in an abrupt step-forcing experiment. The method can be broken down into three steps.

1. The radiative parameters $\mathcal{F}_i, \lambda_i$ are computed by performing a linear fit of ΔN_i against ΔT_i for both the land and the ocean region ($i = l$ and $i = o$) following Gregory et al. (2004). The forcings are the intercepts and the radiative response parameters are the slopes of each regression line.
2. The thermal inertia parameters C_o, C_{do}, γ_o are computed by using two regressions of $\Delta T_o = f(t)$ following Geoffroy et al. (2013a). (see their Sect. 3a). For a step forcing experiment, the ocean surface air temperature response is the sum of a fast response and a slow response. A fit of the 30–150 years of ΔT_o as a function of time is used to compute the slow time scale and the relative amplitude of the slow and the fast responses. The fast time scale is then computed from a fit of the first 15 years of ΔT_o as a function of time. Then analytical relationships are used to compute the three thermal inertia parameters.
3. The horizontal energy transport parameters are computed by performing a linear fit of ΔT_l against ΔT_o . The intercept ΔT_l^{adj} allows to determine α_l and the slope allows to compute α_o (Eq. 11).

In the next section, data from fully coupled atmosphere-ocean general circulation models (AOGCM) experiments are used to validate the LO-EBM framework.

3 Validation and multimodel analysis

3.1 CMIP5 global CO_2 increase experiments

To calibrate and validate the LO-EBM, five experiments of the CMIP5 ensemble (Taylor et al. 2011) are used: piControl (pre-industrial control simulation), abrupt 4xCO_2 (150-year simulation with an abrupt quadrupling of atmospheric CO_2), 1 % year^{-1} CO_2 (140-year simulation with CO_2 increases at 1 % per year until quadrupling after 140 years), SSTClim (fixed SST and sea-ice to their piControl climatological values) and SSTClim4xCO_2 (as SSTClim but with quadrupled CO_2). For a given scenario, the responses (ΔX) are computed by subtracting from the perturbed experiment the corresponding control run: piControl for coupled simulations (by using the time-period of the abrupt 4xCO_2 simulation), and SSTClim for fixed SST runs. For 16 AOGCMs of the CMIP5 ensemble, the parameters of the LO-EBM (calibrated with abrupt 4xCO_2 and piControl) are provided in Table 2. The parameters of the non-linear LO-EBM are given in Table 3.

Figure 1 shows annual mean values of ΔT_l against ΔT_o for each AOGCM and the corresponding LO-EBM fit for the 150 years of the abrupt 4xCO_2 scenario. The linear dependence between the two temperature responses is valid for most of the models. Some climate models exhibit a non-linear behaviour, in particular INMCM4 and FGOALS-s2. Note that FGOALS-s2 and INMCM4 are also outliers in terms of temperature pattern change (Geoffroy and Saint-Martin 2014). All temperature evolutions are well represented with the non-linear LO-EBM (red lines). The intercept at $\Delta T_o = 0$ gives the value of the land fast adjustment temperature ΔT_l^{adj}.

The land fast-adjustment temperature ΔT_l^{adj} is non-negligible with a multimodel mean amplitude of 1.2 K, which corresponds to a small global mean temperature increase of 0.35 K (=1.2f_l). This value obtained by the linear regression is in good agreement with the amplitude obtained in fixed SST experiments (black stars on Fig. 1). Note that in fixed SST experiments, the surface air temperature over the ocean also increases a little, by an average of 0.2 K, as displayed in Fig. 1. Taking into account this increase in the non-linear LO-EBM leads to a land fast response of 1.4 K and 1.1 K for the non-linear LO-EBM estimation (against 1.0 K for the standard non-linear LO-EBM estimation). This improves the consistency with the SSTClim4xCO_2 experiment for most models (and for all models for the non-linear LO-EBM estimation). The differences may also be due to the small heat capacity of the land that is not strictly zero. In the regression method, a non-zero land heat uptake would bias the estimated land fast response to a lower value in comparison with that of the SSTClim4xCO_2 experiment, where the land is in equilibrium. However, the differences between the two estimations are very small.

Figure 2 compares for each model the (ΔN_i, ΔT_i) plots for the AOGCM results and the linear and non-linear LO-EBM fits. The assumption of linear dependence between the radiative response and the surface temperature response is generally valid for each region (grey and black lines). Some limitations are apparent in particular over the ocean for some models (CSIRO-Mk3.6.0, GISS-E2-R, HadGEM2-ES, MPI-ESM-LR, NorESM1-M). These models are characterized by a large efficacy of deep ocean heat uptake (Geoffroy et al. 2013b). The non-linear LO-EBM (blue and red lines) well represents all (ΔN_i, ΔT_i) evolutions, including those characterized by a non-linear behaviour.

In each plot, the vertical line gives the value of the land fast-adjustment temperature estimated with the linear (dashed black) or non-linear fit (dashed red). The intercept between these lines and with the corresponding LO-EBM land response gives the land-stratosphere-troposphere adjusted radiative forcing i.e. the sum of the stratosphere-troposphere adjusted radiative forcing and the land fast radiative restoring. This is directly comparable to the adjusted forcing estimated from the SSTClim experiment

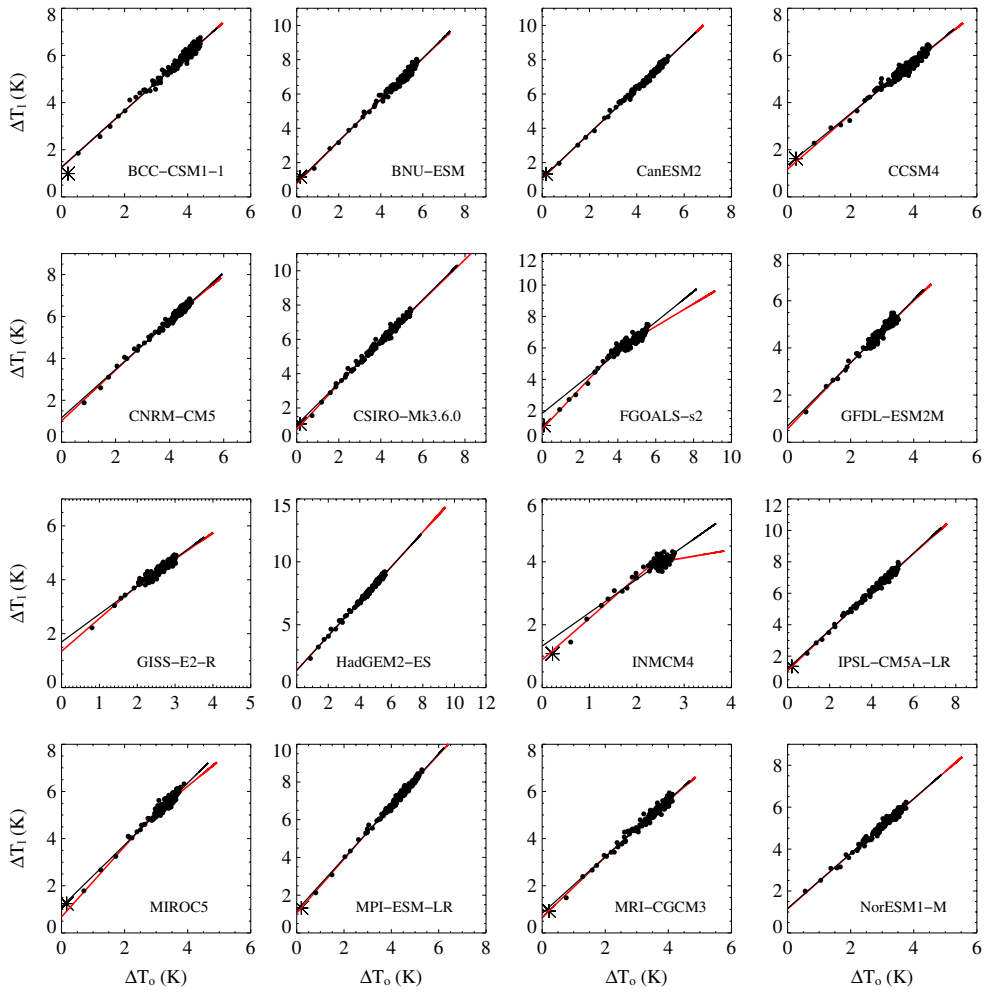

Fig. 1 Mean surface air temperature change over land ΔT_l as a function of the mean surface air surface temperature change over ocean ΔT_o for the abrupt 4xCO_2 experiments (*black dots*, annual mean), for 16 AOGCMs. The *black line* is the linear LO-EBM fit. The *red line* is the non-linear LO-EBM fit. *Black stars* represent the value of (ΔT_l, ΔT_o) from fixed-SST experiments

(red star) (assuming that the ocean temperature response is zero). The land-stratosphere-troposphere adjusted forcing, for the land, and the stratosphere-troposphere adjusted forcing, for the ocean, given by the SSTClim experiment are generally larger than that predicted by the linear LO-EBM.

By taking into account the non-linear behaviour, the forcings over land and ocean are in better agreement. Indeed, first the LO-EBM is consistent with the AOGCM, second the forcings are closest to those calculated from the SSTClim experiment. The reason for this bias would need more investigation. The SSTClim predicts generally slightly larger land forcings and larger land adjusted temperatures than that obtained by regression. Note that by correcting the increase of the 2-m temperature over ocean, the difference of the land fast temperature response between the SSTClim and the regression method would be reduced, as discussed above, but the difference in the forcing would increase.

For a zero heat capacity of the land, the radiative imbalance over land ΔN_l is equal to the land-to-ocean energy transport ΔA. Initially the HET is large. The heat transport is efficient at redistributing energy, preventing the land from significantly warming. Then ΔA decreases until its equilibrium value (intercept of the fit with the vertical dotted line), which is either positive or negative, depending on the climate model. Note that some models exhibit already a negative land-to-ocean HET after 150 years of simulation (CanESM2, CSIRO-Mk3.6.0, GISS-E2-R, IPSL-CM5A-LR).

Figure 3 displays the temporal evolution of the land-sea warming ratio in abrupt 4xCO_2 (used for parameters calibration) and 1 % year^{-1} CO_2 (not used for parameters calibration) experiments, for each individual model and the multimodel mean. The LO-EBM well represents the transient warming over land and ocean in both experiments. The land-sea warming ratio is larger under a

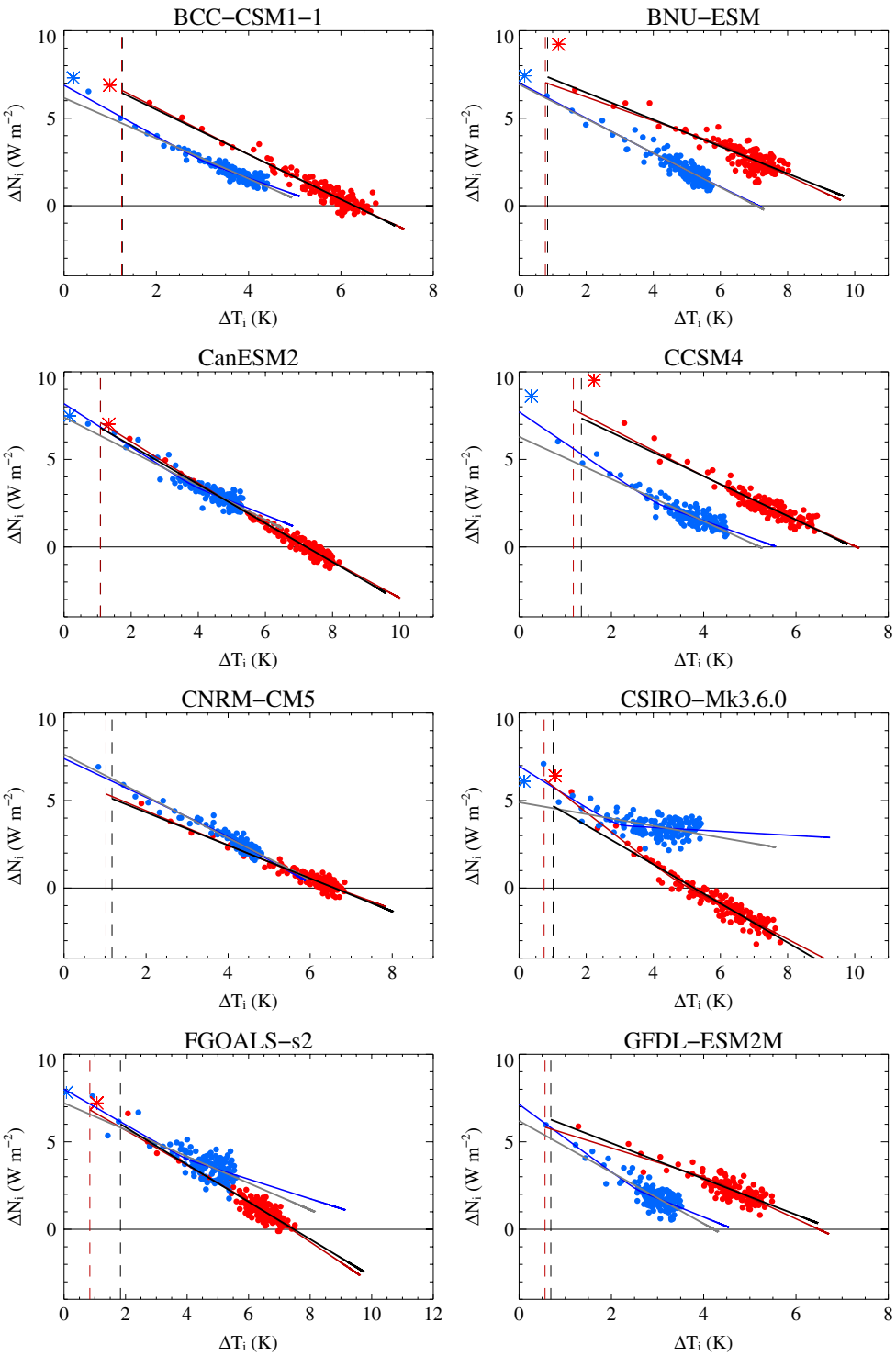

Fig. 2 Net radiative imbalance ΔN_i over land (*red*) and over ocean (*blue*) as a function of the mean surface air temperature change ΔT_i over land (*red*) and ocean (*blue*) for the abrupt 4xCO_2 experiments (*dots*, annual mean), for 16 AOGCMs. The *black* and *grey lines* are the linear LO-EBM fit for land and ocean respectively. The *red* and *blue lines* are the non-linear LO-EBM fit for land and ocean, respectively. The land fast-adjustment temperature is indicated by the *dashed vertical line* for the linear LO-EBM (*black*) and the non-linear LO-EBM (*red*). *Red* and *blue stars* represent the value of (ΔT_l, ΔN_l) and (ΔT_o, ΔN_o), respectively, in fixed-SST experiments

1 % year^{-1} CO_2 simulation than under an abrupt experiment (with respective values of ϕ of 1.55 and 1.49 at t = 140 year) because the climate system is further from its equilibrium state in the 1 % year^{-1} CO_2 simulation than in the abrupt 4xCO_2 simulation. The small amplitude of ΔT_l^{adj} in comparison with ΔT_o means that the second RHS term in Eq. 13 is small after a few years of simulation. This results in a fast decrease of ϕ over the first few years followed by a slow decrease of the land-sea contrast until equilibrium. As a result, it appears as nearly-invariant at the scale of a few decades. The effect of the ocean heat uptake on ϕ is discussed in more detail in Sect. 4.1.

Fig. 2 continued

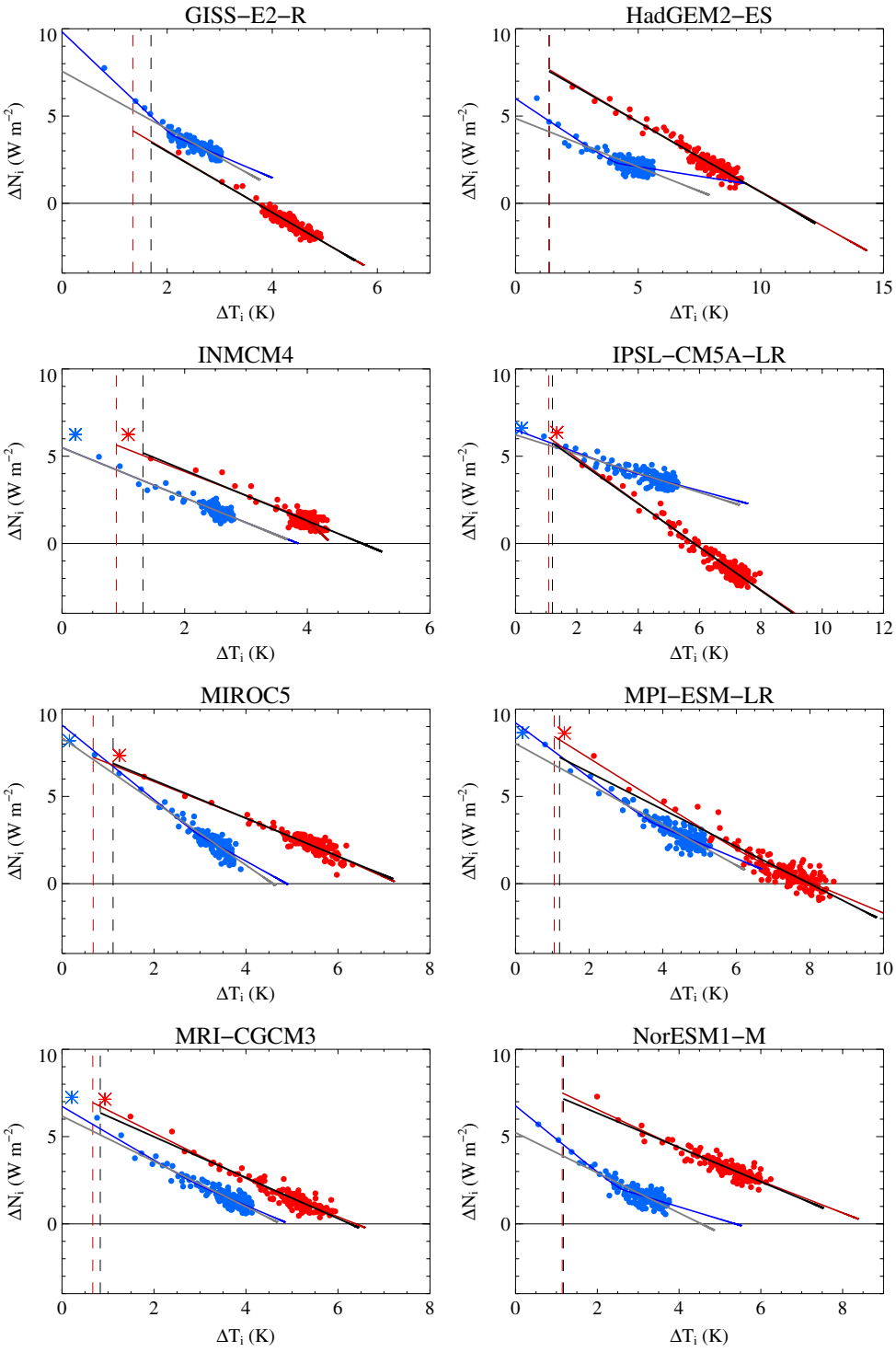

The representation of ΔT_l and ΔT_o is similar (not shown) to that obtained with a global two-layer EBM combined with a pattern scaling decomposition (Geoffroy and Saint-Martin 2014). In comparison with a global EBM combined with a pattern scaling framework, the LO-EBM provides a more general description of the land and ocean responses. In the LO-EBM, the land-sea warming ratio is not constant but depends on the magnitude of the external perturbations over land and ocean and depends on time. To go a step further in the validation, we investigate in the next section the case of heterogeneous perturbations, by considering the extremes scenarios where CO_2 is increased over one single region.

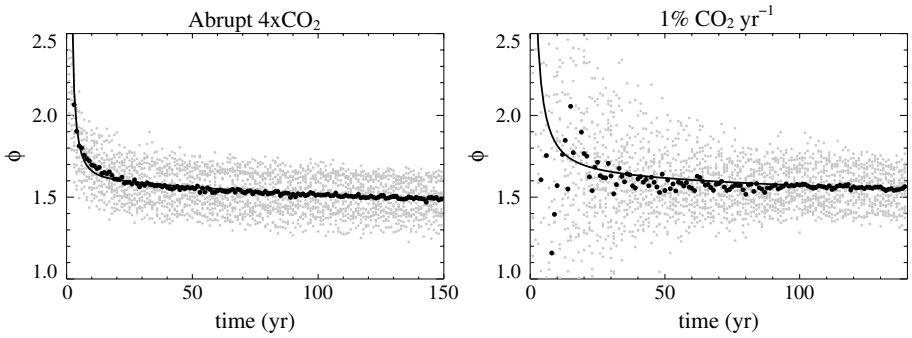

Fig. 3 Temporal evolution of the land sea-warming ratio in abrupt $4xCO_2$ (*left*) and 1 % $year^{-1}$ CO_2 (*right*) experiments, for the multimodel mean (annual means, *black dots*), for each individual model (annual means, *grey dots*) and the multimodel mean of the LO-EBM (*black line*)

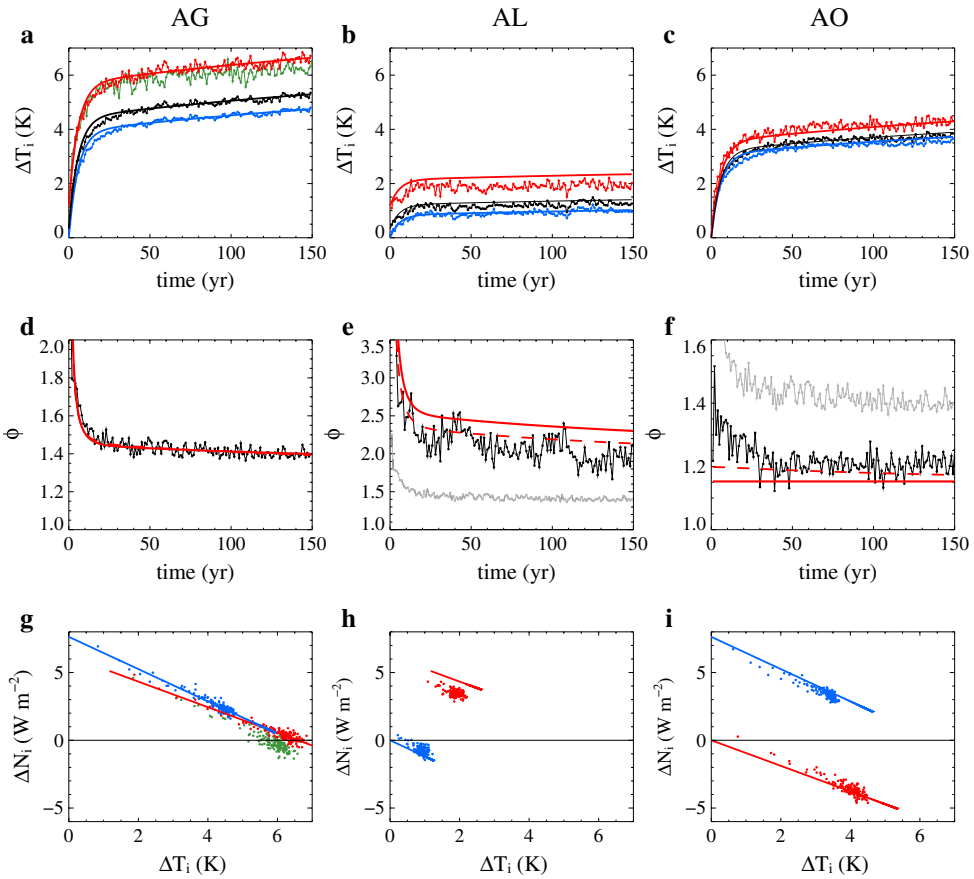

Fig. 4 *Top* Temporal evolution of ΔT_g (*black*), ΔT_l (*red*) and ΔT_o (*blue*) in the AG (**a**), AL (**b**) and AO (**c**) experiments for the CNRM-CM model (*solid lines with dots*) and for the LO-EBM (*solid lines*). The *green solid line* in panel **a** shows the sum of the land-mean surface temperature changes of AL and AO experiments. *Middle* Temporal evolution of the land-sea warming ratio in the AG (**d**), AL (**e**) and AO (**f**) experiments for the CNRM-CM model (*black lines with dots*) and for the linear (*solid red line*) and non-linear LO-EBM (*solid dashed line*). In the **e**, **f** plots, the temporal evolution of φ in the AG experiment is plotted in *grey solid lines*. *Bottom* Net radiative imbalance ΔN_i over land (*red*) and over ocean (*blue*) as a function of surface temperature change over ΔT_i land (*red*) and ocean (*blue*) in the AG (**g**), AL (**h**) and AO (**i**) experiments for the CNRM-CM model (*dots*) and for the LO-EBM fit (*solid lines*). The *green dots* in panel **g** correspond to the sum of the land responses of the AL and AO experiments

3.2 Heterogeneous perturbations experiments

We perform idealized experiments with the CNRM-CM5 climate model (Voldoire et al. 2013) in addition to the global abrupt $4xCO_2$ experiment (referred to hereafter as the AG simulation). In these experiments, an abrupt quadrupling of CO_2 is imposed either only over land (AL simulation) or only over ocean (AO simulation) and is maintained over 150 years. Similar simulations in equilibrium were performed by Forster et al.

(2000) with a intermediate GCM coupled to a mixing layer ocean.

Figure 4a compares the mean surface temperature response $\Delta T_i^{(AG)}$ of the AG experiment to the sum of the global-mean surface temperature responses, $\Delta T_i^{(AO)} + \Delta T_i^{(AL)}$, of the AO and AL experiments, over the whole area, the land and the ocean. Despite a slight difference, the additivity of the responses is verified among the 150 years of the climate transition in agreement with the results of Forster et al. (2000). Figure 4b, c show the temporal evolution of ΔT_g (black), ΔT_l (red) and ΔT_o (blue) for the AL and AO experiments, respectively. The global warming is the largest in the AG experiment and the smallest in the AL experiment, which can be explained by a smaller total radiative forcing in the AL experiment. This result is consistent with that of Forster et al. (2000): the magnitude of the global warming depends in a first approximation to the amplitude of the global forcing, whatever its spatial distribution.

As found by previous authors, the temperature increases in each region for all experiments. The warming over a given region is not only a local response to the forcing, because the energy is redistributed by large-scale advective motions. Indeed, the anomalous land-to-ocean horizontal energy transport ΔA is positive in the AL experiment and negative in the AO experiment (see red dots in Fig. 4h, i). Figure 4d–f show the temporal evolution of the land-sea ratio for the AG, AL and AO experiments, respectively. In all simulations, the land-sea warming ratio is larger than one. ϕ is close to 1.4 in the AG simulation, 2.0 in the AL simulation and 1.2 in the AO simulation. These orders of magnitude are consistent with those obtained in previous studies (Forster et al. 2000; Dommenget 2009) and are discussed in more detail in Sect. 4.1.

The linear and the non-linear LO-EBM analytical solutions are also displayed in Fig. 4. The linear LO-EBM reproduces these variations with a very good agreement. The value of ϕ is overestimated in the AL simulation. Note that this bias is reduced with the non-linear version. Moreover, this bias is associated with a small absolute error for $\Delta T_l^{(AL)}$ that is of the same order as the difference between $\Delta T_l^{(AG)}$ and $\Delta T_l^{(AO)} + \Delta T_l^{(AL)}$. The additivity of the response is not perfectly valid over the land (see Fig. 4a), highlighting a limitation of the framework. Note that the additivity of the response is well verified over the ocean (not shown). In the AO simulation, the land fast adjustment is zero, and the land temperature ΔT_l increases at the same time scale as ΔT_o. The quasi time invariant land-sea ratio is well reproduced despite a slight underestimation at the beginning of the simulation. This may be due to the fact that the land heat capacity is not strictly equal to zero or to oversimplification of mechanisms in the LO-EBM such as land-sea energy transport.

The evolution of the radiative imbalance against the temperature response in each region is also well reproduced by the LO-EBM for both experiments except that there is still a slight overestimation over land in the AL experiment (Fig. 4h). As for the temperature response, the bias is of the same order as the difference between the response to the globally perturbed experiment and the sum of the responses to the decomposed perturbations showing limitation of the assumption of additivity. This slight difference may arise from second-order terms playing a role in the land radiative response. Apart from this small bias, the good correspondence suggests that the representation of the radiative responses as a function of only regional temperature is valid for a land-ocean decomposition.

Other types of idealized experiments, with imposed SST change or imposed land surface temperature change, have been performed in the literature (Compo and Sardeshmukh 2009; Dommenget 2009, 2012; Lambert et al. 2011). For a fixed SST increase with an amplitude equal to 3 K, the linear LO-EBM predicts for a CO_2 concentration maintained at the pre-industrial level and for a doubling of CO_2, a multimodel mean land temperature increase of 3.6 K and 4.8 K and a multimodel mean land-sea warming ratio of 1.2 and 1.6, respectively. These orders of magnitude are in agreement with previous studies (Lambert et al. 2011; Dommenget 2009). For a fixed land temperature increase of 1 K, the multimodel mean equilibrium ocean response is of about 0.5 K, in good agreement with that displayed in the simulations of Dommenget (2012). Finally, the temperature and radiative responses in idealized experiments, such as the AL and AO experiments, are well reproduced by the LO-EBM calibrated with only the AG experiments. In particular the land-sea warming ratio varies in these experiments and this feature is well predicted by the LO-EBM. These results instill confidence in the framework and the method of calibration used. In the following section, the LO-EBM is used to investigate the role of each mechanism in the land-sea warming contrast.

4 Role of the horizontal energy transport and other mechanisms

4.1 Magnitude of the land-sea warming ratio

In this section, the role of the different parameters (forcing amplitudes, radiative response parameters, HET parameters and thermal inertia parameters) at play in the land-sea warming contrast is analysed in equilibrium and in transition. From Eqs. (8) and (9), the land and ocean equilibrium temperature responses and the equilibrium land-sea ratio read:

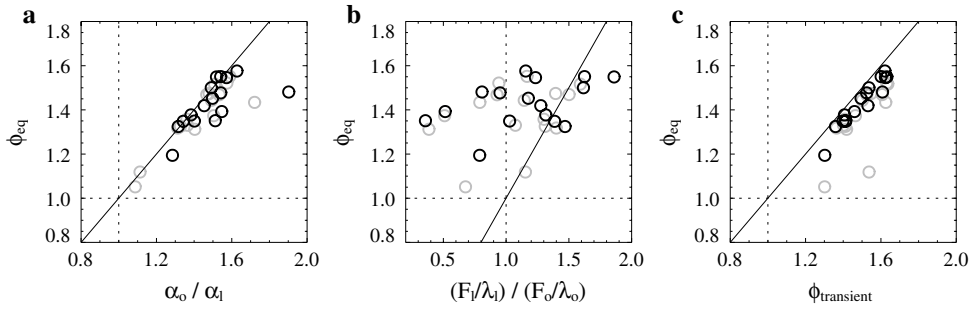

Fig. 5 **a** LO-EBM equilibrium land-sea warming ratio as a function of **a** the ratio of the HET coefficients, **b** the ratio of the local radiative equilibrium temperature responses and **c** the transient land-sea warming ratio defined as the mean over the last 20 years of the 4xCO_2 experiment. The *black solid line* shows the 1:1 line. The *dotted lines* represents the $y = 1$ and $x = 1$ lines

Table 2 The parameter estimates in the framework of the linear LO-EBM of the 16 CMIP5 models used in this paper, and their multimodel mean and SD

	$\mathcal{F}_l$	$\mathcal{F}_o$	λ_l	λ_o	α_l	α_o	C_o	C_{do}	γ_o
BCC-CSM1-1	8.0	6.2	1.28	1.15	1.48	2.21	13	146	2.04
BNU-ESM	8.0	6.9	0.77	0.98	2.51	3.31	12	264	1.97
CanESM2	8.0	7.4	1.11	0.98	1.81	2.80	12	186	1.90
CCCSM4	9.0	6.3	1.25	1.21	1.58	2.12	11	160	2.15
CNRM-CM5	6.2	7.6	0.94	1.19	1.27	1.77	14	301	2.19
CSIRO-Mk3.6.0	5.8	4.9	1.12	0.34	1.34	2.03	10	128	1.78
FGOALS-s2	8.0	7.2	1.06	0.76	0.95	1.22	11	310	2.22
GFDL-ESM2M	7.0	6.2	1.02	1.47	2.65	3.94	14	227	1.93
GISS-E2-R	6.4	7.6	1.74	1.65	0.60	1.14	8	252	2.56
HadGEM2-ES	8.7	4.9	0.80	0.56	1.61	2.53	12	219	1.79
INMCM4	7.1	5.5	1.45	1.43	1.14	1.66	14	673	2.30
IPSL-CM5A-LR	7.3	6.2	1.24	0.55	1.39	2.15	13	204	1.83
MIROC5	8.1	8.4	1.09	1.82	1.80	2.77	14	305	2.12
MPI-ESM-LR	8.5	8.0	1.06	1.16	1.75	2.85	13	167	1.90
MRI-CGCM3	7.3	6.2	1.17	1.30	2.22	3.07	13	162	2.02
NorESM1-M	8.3	5.2	0.95	1.15	1.77	2.69	14	199	1.96
Multimodel mean	7.6	6.5	1.13	1.11	1.62	2.39	12	244	2.04
SD	0.9	1.1	0.24	0.41	0.54	0.75	2	128	0.21

$\mathcal{F}_i$ are expressed in W m^{-2}, λ_i, α_i and γ_o in W m^{-2}K^{-1} and C_o and C_{do} in W y m^{-2}K^{-1}

$$\Delta T_l^{eq} = \left[\left(\lambda_o + \frac{\alpha_o}{1-f_l}\right)\mathcal{F}_l + \frac{\alpha_o}{f_l}\mathcal{F}_o\right] \Big/ \left[\lambda_l\lambda_o + \lambda_l\frac{\alpha_o}{1-f_l} + \lambda_o\frac{\alpha_l}{f_l}\right], \tag{15}$$

$$\Delta T_o^{eq} = \left[\frac{\alpha_l}{1-f_l}\mathcal{F}_l + \left(\lambda_l + \frac{\alpha_l}{f_l}\right)\mathcal{F}_o\right] \Big/ \left[\lambda_l\lambda_o + \lambda_l\frac{\alpha_o}{1-f_l} + \lambda_o\frac{\alpha_l}{f_l}\right], \tag{16}$$

$$\phi^{eq} = \frac{\left[\lambda_o + \frac{\alpha_o}{1-f_l}\right]\mathcal{F}_l + \frac{\alpha_o}{f_l}\mathcal{F}_o}{\frac{\alpha_l}{1-f_l}\mathcal{F}_l + \left[\lambda_l + \frac{\alpha_l}{f_l}\right]\mathcal{F}_o}. \tag{17}$$

In the case of zero horizontal energy transport ($\alpha_o = \alpha_l = 0$), ϕ^{eq} would be equal to the ratio of the local radiative equilibrium temperature responses, i.e.

$$\phi^{eq}|_{\{\alpha_i=0\}} = \frac{\mathcal{F}_l}{\lambda_l}\frac{\lambda_o}{\mathcal{F}_o} \tag{18}$$

Figure 5a shows that the ratio of these local radiative equilibrium temperature responses is smaller than the equilibrium land-sea warming ratio. The local radiative equilibrium temperature response over the land is even smaller than that over the ocean for some models, showing that the geographical differences in the forcing adjustment and in the strength of the radiative feedbacks are not the main drivers of the land-sea contrast, which is consistent with previous studies (Joshi et al. 2008).

Table 3 The parameter estimates in the framework of the non-linear LO-EBM of the 16 CMIP5 models used in this paper, and their multimodel mean and SD

	$\mathcal{F}_l$	$\mathcal{F}_o$	λ_l	λ_l^D	λ_o	λ_o^D	α_l	α_l^D	α_o	α_o^D	C_o	C_{do}	γ_o
BCC-CSM1-1	8.2	6.9	1.30	1.24	1.24	0.92	1.53	1.43	2.29	2.13	15	86	1.06
BNU-ESM	7.6	7.0	0.76	0.90	0.98	0.95	2.61	2.35	3.42	3.09	12	125	0.94
CanESM2	8.3	8.2	1.12	1.05	1.03	0.76	1.91	1.75	2.92	2.69	13	115	1.04
CCCSM4	9.4	7.7	1.28	1.19	1.38	0.93	1.94	1.36	2.57	1.80	13	112	1.29
CNRM-CM5	6.3	7.4	0.94	0.87	1.18	1.32	1.52	0.91	2.08	1.24	13	127	0.95
CSIRO-Mk3.6.0	7.1	7.0	1.16	0.99	0.44	0.09	2.42	1.57	3.40	2.20	14	111	1.26
FGOALS-s2	7.7	8.0	1.08	1.18	0.75	0.55	2.36	0.65	2.56	0.70	12	193	1.19
GFDL-ESM2M	6.4	7.1	0.99	1.22	1.54	1.05	3.02	2.35	4.46	3.47	15	183	1.37
GISS-E2-R	6.5	9.8	1.75	1.73	2.09	1.26	0.90	0.65	1.54	1.12	11	209	1.84
HadGEM2-ES	8.8	6.0	0.80	0.78	0.52	0.21	1.60	1.62	2.51	2.55	13	138	0.90
INMCM4	7.0	5.5	1.58	3.32	1.43	1.41	1.85	0.28	2.06	0.31	15	382	1.17
IPSL-CM5A-LR	7.4	6.5	1.25	1.20	0.56	0.47	1.63	1.34	2.46	2.01	13	133	1.13
MIROC5	8.0	9.1	1.09	1.15	1.86	1.45	3.10	0.97	4.54	1.43	15	225	1.36
MPI-ESM-LR	9.6	9.2	1.12	0.87	1.25	0.87	2.33	1.41	3.70	2.24	15	121	1.14
MRI-CGCM3	7.8	6.7	1.21	1.04	1.37	1.11	3.01	1.59	4.10	2.16	15	100	1.10
NorESM1-M	8.6	6.8	1.00	0.91	1.24	0.69	1.90	1.64	2.87	2.48	17	179	1.42
Multimodel mean	7.8	7.4	1.15	1.23	1.18	0.88	2.10	1.37	2.97	1.98	14	159	1.20
SD	1.0	1.2	0.25	0.60	0.46	0.40	0.63	0.57	0.89	0.85	1	73	0.23

$\mathcal{F}_i$ are expressed in W m^{-2}, λ_i, α_i and γ_o in W m^{-2} K^{-1} and C_o and C_{do} in W y m^{-2} K^{-1}

Assuming that the forcing amplitude over land and ocean are equal $\mathcal{F}_l = \mathcal{F}_o$, Eq. (17) becomes:

$$\phi^{eq}|_{\{\mathcal{F}_l=\mathcal{F}_o\}} = \frac{\lambda_o + \alpha_o/(f_l(1-f_l))}{\lambda_l + \alpha_l/(f_l(1-f_l))}. \tag{19}$$

The relative amplitude of $\alpha_i/(f_l(1-f_l))$ is larger than the characteristic value of the radiative response parameter (see Table 2). The ratio α_o/α_l is larger than one and close to ϕ^{eq} (Fig. 5b). Note that, for a given value of λ_o, λ_l, α_o and α_l, the minimum of the land-sea warming ratio occurs for $f_l(1-f_l)$ maximum, hence for $f_l = 0.5$. Finally, the land-sea warming ratio is explained by the asymmetrical dependency of the HET change on the surface temperature responses over land an ocean ($\alpha_o > \alpha_l$), which is in agreement with the study of Joshi et al. (2013).

For a forcing applied only over the land or an imposed land surface temperature ($\mathcal{F}_o = 0$), the equilibrium land-sea warming ratio reads:

$$\phi^{eq}|_{\{\mathcal{F}_o=0\}} = \frac{\lambda_o + \alpha_o/(1-f_l)}{\alpha_l/(1-f_l)} \tag{20}$$

In this case, the land-sea warming ratio does not depend on the amplitude of the land forcing. This explains that both types of experiments lead to a similar land-sea warming ratio. Eq. (20) can be obtained by considering the ocean-area energy budget that consists in a balance between the land-to-ocean HET change and the ocean radiative response. The disappearance of λ_l in the denominator explains why the land-sea ratio is larger in experiments where forcing is applied only over the land than applied globally ($\phi = 2$ and $\phi = 1.4$ at equilibrium in the AL and the AG experiments, respectively).

For a forcing applied only over the ocean or an imposed SST ($\mathcal{F}_l = 0$), the land-sea warming ratio becomes:

$$\phi^{eq}|_{\{\mathcal{F}_l=0\}} = \frac{\alpha_o/f_l}{\lambda_l + \alpha_l/f_l} \tag{21}$$

For a typical value of the parameter, ϕ^{eq} is larger than one. In this case, the radiative response of the land area, which is indicated by the presence of λ_l in the denominator in Eq. (21), acts to reduce the land-sea contrast in comparison with a globally perturbed experiment. If ΔA verified a diffusive law as a function of surface temperature change ($\alpha_o = \alpha_l$), the land-sea warming ratio would be lower than 1 because the negative land radiative response would impose a negative land-to-ocean HET change. On the contrary, the asymmetry in the relative surface area covered by the land and the ocean ($f_l < 0.5$) tends to increase in this case the land-sea warming ratio. Indeed, the larger the ocean area is, the more the land receives energy per unit of land area. If the land fraction was 0.5 and the other parameters remained unchanged, ϕ^{eq} would be lower than one for four CMIP5 models over 16. Hence in a fixed SST experiment, the land-sea warming ratio is robustly positive due to the asymmetry in the HET change formula and because the forced area is large enough that the HET efficiently counteracts the land radiative response.

Figure 5c shows the transient land-sea warming ratio in an abrupt 4xCO_2 experiment as a function of ϕ^{eq}. All models exhibit a lower land-sea contrast in transition than

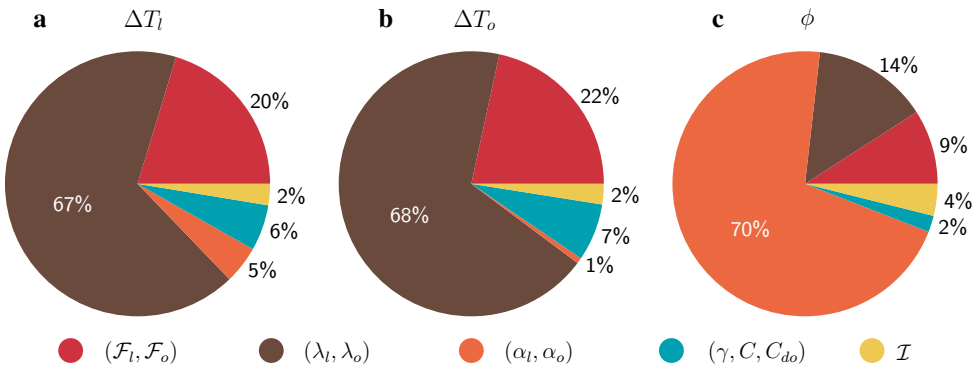

Fig. 6 Pie chart of the contribution (%) of the four groups of parameters to the spread of **a** the surface temperature change over land, **b** the surface temperature change over ocean and **c** the land-sea warming ratio. The contribution of the interaction term is plotted in *yellow*

in equilibrium. This behaviour is consistent with previous studies that show a lower land-sea contrast at equilibrium (from mixing-layer ocean models) than during transition phases. In transition, the ocean heat uptake constitutes a sink of energy in addition to the ocean radiative response. Its effect is equivalent to increasing λ_o in Eq. (17), leading to a larger ϕ in transition than in equilibrium.

Finally, the asymmetry in the value of α_o and α_l explains the land-sea warming contrast in equilibrium. The heat uptake reduces ϕ in transition. The geographical differences in the strength of the radiative feedbacks and that of the forcing adjustment modulate the magnitude of the land-sea warming ratio. In the next section we investigate to what extent the intermodel differences in the strength of each mechanism contribute to the intermodel spread of the land-sea warming ratio in a climate transition.

4.2 Contributions to the spread of the land-sea warming ratio

In this section, we use the linear LO-EBM and the analysis of variance (ANOVA) method to investigate the source of intermodel spread in the land temperature response ΔT_l , the ocean temperature response ΔT_o and the land-sea ratio ϕ. This method is fully described in Geoffroy et al. (2012) (see their Sect. 3). Four groups of parameters are considered: the radiative forcings $(\mathcal{F}_l, \mathcal{F}_o)$, the radiative response parameters (λ_l, λ_o), the thermal inertia parameters (γ_o, C_o, C_{do}) and the HET parameters (α_l, α_o). The spread of each response is analysed in the abrupt $4xCO_2$ experiment after 150 years of integration. The multimodel mean (over the last 30 years of simulation) of ΔT_l, ΔT_o and ϕ are 6.5 K, 4.4 K and 1.5, respectively, with a SD of 1.3 K, 0.9 K and 0.1, respectively. The contribution of each group of parameters to the spread of ΔT_l, ΔT_o and ϕ is given in Fig. 6. In each case, the interaction term $\mathcal{I}$ is verified to be small (3, 3 and 4 % respectively).

Concerning the main contributors to the spread of the temperature responses, both land and ocean exhibit similar results (Fig. 6a, b). The radiative response parameters are the main contributors with a contribution of 67 and 68 %, respectively. The adjustment of the radiative forcing is the second contributor with a contribution of 20 and 22 %, respectively. These results are consistent with those obtained for the spread of the global-mean surface air temperature response (Geoffroy et al. 2012). However, the contributions differ slightly for the thermal inertia and the HET parameters. The thermal inertia parameters contribute more to the spread of ΔT_o (7 %) than to that of ΔT_l (6 %) because the deep-ocean heat uptake directly impacts the ocean temperature response. On the other hand, the HET parameters contribute to 5 % of the spread of ΔT_l whereas their contribution to that of ΔT_o is negligible (1 %). Note that the non-linear LO-EBM leads to a similar conclusion.

The repartition of the source of the spread of the land-sea warming ratio depicts a different picture (Fig. 6c). As expected, both differences in the thermal inertia parameters are small (2 %). The contribution of the feedback parameters is the second contributor, but with a contribution of only 14 %. The forcing contributes to 9 %. The main contributor is the intermodel difference in the HET parameters with a large contribution of 70 %. Note that the HET parameters are determined in the last step of the calibration procedure. Thus, their estimation includes all errors associated with the limitation of the framework and the method of calibration. Their contribution to the spread may be overestimated. However, differences between the relative contribution of the various parameters are so large that the results clearly support that the HET is the main contributor to the amplitude and the multimodel spread of the land-sea ratio.

With the non-linear LO-EBM, the contribution of the HET parameters (α_o, α_l, α_o^d and α_l^d) is increased to 77 % and that of the climate response parameter (λ_o, λ_l, λ_o^d and λ_l^d) is decreased to 6 %. Note that the differences in the results are due to the two outlier models, INMCM4 and FGOALS-s2, for which the behaviour, the validity of the non-linear LO-EBM framework and the calibration method may be questionable. By excluding these models, the results are similar to those obtained with the linear LO-EBM, giving more confidence in the results provided by the linear

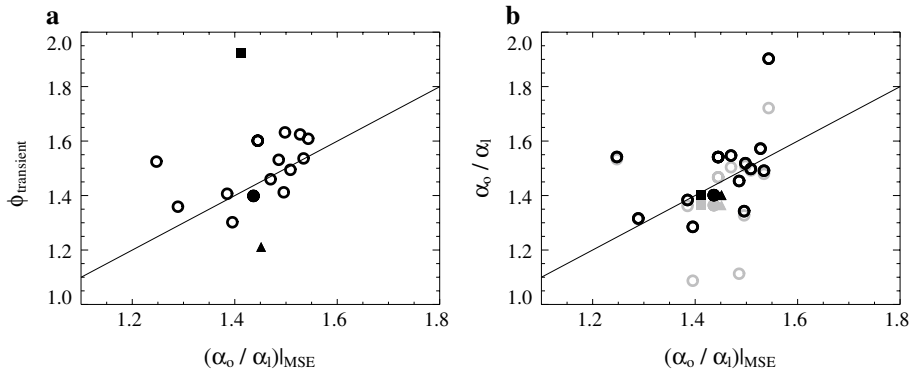

Fig. 7 Land-sea warming ratio (mean over the last 30 years of experiment) as a function of χ (*left*) and ratio of the HET parameters α_o/α_l as a function of χ (*right*). The *circles* show the values of each individual model for AG experiments. The full *symbols* represent the CNRM-CM5 climate model. The *square* and the *triangle* represent the AL and the AO experiment, respectively. On the *right panel*, *black* and *grey symbols* represent estimations of α_o/α_l with the linear LO-EBM and the non-linear LO-EBM, respectively

LO-EBM framework. In the next section the origin of the difference in α_l and α_o is discussed by focusing on the role of the moist static energy difference over the land and the ocean.

4.3 Role of the moist static energy changes in the asymmetry of the HET change

This section discusses the potential causes for differential α_l and α_o by focusing on the role of moist static energy (MSE) change over land and ocean. Joshi et al. (2008) show that the difference in the lapse rate changes over the land and over the ocean due to different humidity supply and similar free tropospheric warming, result in a land-sea warming contrast. From these considerations, Byrne and O'Gorman (2013a, b) develop a tropical theory based on the surface equivalent potential temperature change. For heterogeneous perturbation, such as aerosol forcing, the atmospheric dynamics may not be strong enough to counteract differences in free-troposphere diabatic heating change and smooth the free-troposphere temperature changes (Joshi et al. 2013). To take into account this effect, Joshi et al. (2013) use a simple model that consists of a balance between the diabatic heating and the energy transport in the free troposphere and assumes the latter follows a diffusive formula as a function of lower free-troposphere temperature change. The ideas of Joshi et al. (2013) can be reformulated within the framework of the LO-EBM by considering that the horizontal energy transport ΔA acts to homogenize the moist static energy (MSE) change by following a diffusive law:

$$\Delta A = k(\Delta m_l - \Delta m_o), \tag{22}$$

where k is a diffusive coefficient, $\Delta m_i = C_p \Delta T_i + L_v \Delta q_i$ is the mean surface air MSE response over region i (land or ocean), q_i is the mean surface air specific humidity over region i, C_p is the specific heat capacity of air at constant pressure, and L_v is the latent heat of vaporization of water. This type of diffusive formula based on the MSE change has already been used to represent latitudinal energy transport (Hwang and Frierson 2010; Rose et al. 2014). Assuming Eq. (22), the ratio of the HET parameters $\frac{\alpha_o}{\alpha_l}|_{mse}$ reads (Eq. 7):

$$\frac{\alpha_o}{\alpha_l}|_{mse} = \frac{C_p + L_v \frac{\partial q_o}{\partial T_o}}{C_p + L_v \frac{\partial q_l}{\partial T_l}} = \chi \tag{23}$$

This ratio is larger than one due to the differential increase of the surface specific humidity over the ocean than over the land, this behaviour being that expected for a roughly invariant relative humidity.

In the particular case of zero HET change, Eq. (23) assumes that the MSE changes are equal over the land and the ocean. This corresponds to the hypothesis of Byrne and O'Gorman (2013a, b) applied to the total land and ocean area. In such a case, the land-sea warming ratio is equal to χ. We calculate this ratio for the last 30 years of CMIP5 abrupt 4xCO_2 experiments following Eq. (23), by computing $\frac{\partial q_i}{\partial T_i}$ as the ratio of Δq_i (the mean surface air specific humidity change over region i) to ΔT_i. Figure 7a shows a good correspondence between χ and ϕ in CMIP5 abrupt 4xCO_2 experiments. This suggests that the hypotheses of Joshi et al. (2008) and Byrne and O'Gorman (2013a, b) give reasonable results at the global scale for homogeneous forcing experiments. However, the relationship is not verified for the CNRM-CM AL and AO experiments (square and triangle in Fig. 7), in which the HET change is far from zero (Fig. 4h, i), confirming the ideas of Joshi et al. (2013).

To investigate the validity of Eq. 23, the ratio of the HET parameters given by the linear LO-EBM is compared

to χ for the CMIP5 models abrupt 4xCO_2 experiment and CNRM-CM AL and AO experiments (Fig. 7b). The equality between α_o/α_l and χ is valid for almost all models (except two outliers, GISS-E2-R and CCCSM4). With the non linear LO-EBM (grey circles), the correspondence is generally improved except for the two outliers pointed out in previous sections, INMCM4 and FGOALS-s2, for which large differences emerge, revealing limitations in the LO-EBM framework and in the method used to determine α_o and α_l. A remarkable feature displayed in Fig. 7b is the invariance of χ in the homogeneous forcing (AG) and heterogeneous forcing (AL and AO) CNRM-CM5 experiments (full symbols), whereas the land-sea warming ratio strongly differs in these simulations. These results suggest that the hypothesis that the HET change obeys a diffusive law as a function of surface MSE change is valid to the first order, hence explaining most of the differences in α_o and α_l.

The differential moist static energy responses over land and ocean can be estimated from the mean preindustrial state from Clausius-Clapeyron scaling, by assuming constant relative humidity over land and ocean (Held and Soden 2006). However, such an assumption is limited. The multimodel mean value of χ obtained by assuming constant relative humidity is lower than the multimodel mean value of α_o/α_l given by the LO-EBM (1.3 and 1.5, respectively). Moreover, the equality between individual values is not verified. In particular, we find that this limitation is due to significant changes in the relative humidity over the land for some models (not shown), in agreement with the results of Byrne and O'Gorman (2013b). Moreover, the use of the diffusive formula for the HET change given by Eq. (22) does not well represent the transient land and ocean temperature responses for all models (not shown). Hence additional mechanisms have to be taken into account to explain the asymmetry in α_o and α_l.

Different factors may contribute to these differences, beyond the use of the surface MSE change to represent the free-troposphere conditions change at the global scale. In particular, the smoothing of the free-troposphere temperature is efficient zonally (Joshi et al. 2013; Byrne and O'Gorman 2013a) but may be counteracted by latitudinal variations in diabatic heating. Hence, the spatial distribution of the MSE changes, and therefore the pattern of the temperature and the humidity changes, may play a role in addition to the strength of the local HET change in terms of space-variation of the diffusive coefficient. More investigation would be necessary to attribute the differences between the HET parameters and to relate the changes in the strength of the HET to the preindustrial state.

5 Summary and conclusion

In this article, we have investigated the role of the different mechanisms at play in the land-sea warming contrast and the CMIP5 intermodel spread of the land-sea warming ratio by using an energy-balance model framework. To this end, we have developed an energy-balance model with one box representing the land and two boxes representing the near-surface and the deeper ocean. The HET change between the two upper boxes is parameterized as a linear function of the land and the ocean mean surface air temperature responses by using two distinct heat exchange coefficients rather than a single coefficient as is the case for a diffusive law. A more sophisticated version of this EBM with three additional parameters has also been developed to take into account non-linear behaviours associated with the deep-ocean heat uptake, which act as an additional forcing for the near-surface ocean layer in transition. A method of calibration of the LO-EBM parameters from an abrupt CO_2 forcing experiment have been presented.

Once calibrated with an abrupt 4xCO_2 experiment, the LO-EBM is able to represent the land and ocean temperature responses, and the land-sea warming ratio, in equilibrium and in transient conditions for different types of idealized experiments and forcing scenarios. The simple model has been shown to well represent the land response in fixed SST experiments with CO2 quadrupling, the time evolution of the land-sea warming ratio in atmosphere-ocean coupled experiments, and its variations associated with heterogeneous perturbations (forcing over land or ocean only). The model also reproduces the order of magnitude found in the literature for experiments such as fixed SST increase or fixed land surface temperature increase.

Under the LO-EBM framework, the mean surface air temperature response over the land and ocean is the result of a balance between the local radiative forcing, the radiative response associated with the local temperature increase, the HET change between the land and the ocean area and, in a climate transition, the ocean heat-uptake. The results presented in this study suggest that the magnitude of the land-sea warming ratio is mainly explained by the HET, consistent with the previous study of Joshi et al. (2013). It is modulated by the strength of the land and ocean radiative responses and forcing adjustments that, taken alone, would impose a land-sea warming ratio either larger or lower than one, depending on the climate model. In transition, the land-sea warming ratio is increased by the deep-ocean heat uptake. Whereas the radiative response parameters and to a lesser extent the forcing adjustments are the main contributors to the CMIP5 intermodel spread in both land and ocean temperature responses, the HET is found to be the main contributor to the intermodel spread in the magnitude

of the land-sea warming ratio (with a contribution of about 70 % of the spread). The strength of the radiative mechanisms constitutes the second contributor to this spread, whereas the role of the thermal inertia is small.

The land-sea warming contrast arises from the asymmetric dependency of the HET on the land and the ocean temperature responses. The order of magnitude of these differences is consistent with the theory that the HET follows a diffusive law as a function of the mean surface air MSE change. However, such a law is not enough to explain the intermodel differences in the HET parameters and some climate models' behaviour. In addition the relative humidity may vary significantly for some models, in particular above the land, which create deviation from Clausius-Clapeyron scaling. More investigation is necessary to relate the HET parameters to the physical processes at play in the HET. In this aim, an analysis of tropospheric quantities and their relationship with surface conditions and in particular the role of humidity need to be investigated. The framework presented here may help such an analysis by providing parameters representative of ensemble properties of the climate system at play in the land-sea contrast.

Finally, one possible future development of this work is to investigate the validity of the LO-EBM for other forcings (aerosols, natural) in order to study the 20th Century evolution. Another perspective concerns the extension of this framework to other spatial decompositions of the climate system such as zonal decomposition. Pattern scaling studies of the temperature response suggest that linear behaviours are valid regionally, hence linear parameterization of the HET should remain valid. However, in other types of spatial decomposition, additional heat capacities are involved, hence necessitating the analysis of regional heat-uptake. Moreover, the extent to which the concept of local feedback is valid at finer spatial decomposition and the relative role of remote feedbacks and their representation remain to be addressed.

Acknowledgments We gratefully thank two anonymous reviewers for their constructive comments and suggestions that helped to improve the manuscript. We also thank Laura Watson for comments on the manuscript and Bjorn Stevens for an inspiring discussion on this topic. This work was supported by the Project MORDICUS. We acknowledge the World Climate Research Programme's Working Group on Coupled Modelling, which is responsible for CMIP, and the U.S. Department of Energy's Program for Climate Model Diagnosis and Intercomparison which provides coordinating support and led development of software infrastructure in partnership with the Global Organization for Earth System Science Portals. We thank the climate modeling groups for producing and making available their model output.

Conflict of interest The authors declare that they have no conflict of interest.

Appendix

Non-linear LO-EBM

As in Held et al. (2010) and Geoffroy et al. (2013b), two additional climate response parameters, λ_o^d and λ_l^d (which can be related to that associated with the CO_2 forcing with an efficacy factor), and two HET parameters, α_o^d and α_l^d, are introduced to take into account the non-linear evolutions:

$$0 = \mathcal{F}_l - \lambda_l\left(\Delta T_l - \Delta T_l^d\right) + \frac{\alpha_o}{f_l}\left(\Delta T_o - \Delta T_o^d\right) - \frac{\alpha_l}{f_l}\left(\Delta T_l - \Delta T_l^d\right) \tag{24}$$

$$0 = -\lambda_l^d \Delta T_l^d + \frac{\alpha_o^d}{f_l}\Delta T_o^d - \frac{\alpha_l^d}{f_l}\Delta T_l^d, \tag{25}$$

$$C_o\frac{d\Delta T_o}{dt} = \mathcal{F}_o - \lambda_o\left(\Delta T_o - \Delta T_o^d\right) - \frac{\alpha_o}{1-f_l}\left(\Delta T_o - \Delta T_o^d\right) + \frac{\alpha_l}{1-f_l}\left(\Delta T_l - \Delta T_l^d\right) \tag{26}$$

$$0 = -\lambda_o^d \Delta T_o^d - \frac{\alpha_o^d}{1-f_l}\Delta T_o^d + \frac{\alpha_l^d}{1-f_l}\Delta T_l^d - \gamma(\Delta T_o - \Delta T_{do}). \tag{27}$$

where ΔT_o^d and ΔT_l^d are the mean surface air temperature responses associated with the deep-ocean heat-uptake, over the ocean and over the land, respectively.

By adding Eqs. 24 and 25 and using Eqs. 27 and 28, the system of equations for ΔT_o reads:

$$C_o\frac{d\Delta T_o}{dt} = \mathcal{F}_o^* - \lambda_o^*\Delta T_o - \gamma_o^*(\Delta T_o - \Delta T_{do}), \tag{28}$$

$$C_{do}^*\frac{d\Delta T_{do}}{dt} = \gamma_o^*(\Delta T_o - \Delta T_{do}) \tag{29}$$

with:

$$\mathcal{F}_o^* = \mathcal{F}_o + \frac{\alpha_l}{1-f_l}\Delta T_l^{adj} \tag{30}$$

$$\lambda_o^* = \lambda_o + \frac{\alpha_o}{1-f_l} - \frac{\alpha_l}{1-f_l}\frac{\alpha_o/f_l}{\lambda_l + \alpha_l/f_l} \tag{31}$$

$$\lambda_o^{d*} = \lambda_o^d + \frac{\alpha_o^d}{1-f_l} - \frac{\alpha_l^d}{1-f_l}\frac{\alpha_o^d/f_l}{\lambda_l^d + \alpha_l/f_l} \tag{32}$$

$$\gamma_o^* = \gamma_o\frac{\lambda_o^*}{\lambda_o^{d*}} \tag{33}$$

$$C^*_{do} = C_{do}\frac{\lambda^*_o}{\lambda^{d*}_o} \tag{34}$$

The analytical solution of this system for an abrupt and a linear forcing is given in Geoffroy et al. (2013a, b).

From Eqs. 24 and 25, the land surface air temperature response ΔT_l reads:

$$\Delta T_l = \Delta T_l^{adj} + \frac{\alpha_o/f_l}{\lambda_l + \alpha_l/f_l}(\Delta T_o - \Delta T_o^d) + \frac{\alpha_o^d/f_l}{\lambda_l^d + \alpha_l^d/f_l}\Delta T_o^d, \tag{35}$$

The formula of ΔT_l^{adj} is unchanged (but the values of the parameters are different) and the formula of ϕ has an additional term.

The calibration of the parameters is performed iteratively by using the linear LO-EBM as initial values. Then, the following iterations are performed in three steps:

1. The radiative parameters $\mathcal{F}_l, \lambda_l, \lambda_l^d, \mathcal{F}_o, \lambda_o, \lambda_o^d$ are computed from a multilinear regression of ΔN_i against ΔT_i (value of the climate model) and ΔT_i^d (analytical solution) for the land and the ocean region ($i = l$ and $i = o$, respectively).
2. The thermal inertia parameters C_o, C_{do} and γ_o are calculated from two fits of ΔT_o against time as in Geoffroy et al. (2013a) and Geoffroy et al. (2013b).
3. The HET parameters are computed by multilinear regression of ΔT_l against $(\Delta T_o - \Delta T_o^d)$ and ΔT_o^d. Equation 35 can be written as the following:

$$\Delta T_l = \Delta T_l^{adj} + k_{eq}(\Delta T_o - \Delta T_o^d) + k_d(\Delta T_o^d). \tag{36}$$

Hence, the intercept of the multilinear regression gives α_l (Eq. 12) then k_{eq} gives α_o (Eq. 35) and α_l^d and α_o^d are computed from k_d by assuming $\alpha_l/\alpha_o = \alpha_l^d/\alpha_o^d$.

References

Bates JR (1999) A dynamical stabilizer in the climate system: a mechanism suggested by a simple model. Tellus A 51:349–372

Bates JR (2007) Some considerations of the concept of climate feedback. Q J R Meteorol Soc 133:545–560

Beltrami H, Smerdon J, Pollack H, Huang S (2002) Continental heat gain in the global climate system. Geophys Res Lett 29:1167

Boer GJ, Yu B (2003) Climate sensitivity and response. Clim Dyn 20:415–429

Byrne MP, O'Gorman PA (2013a) Land-ocean warming contrast over a wide range of climates: convective quasi-equilibrium theory and idealized simulations. J Clim 26:4000–4016

Byrne MP, O'Gorman PA (2013b) Link between land-ocean warming contrast and surface relative humidities in simulations with coupled climate models. Geophys Res Lett 40:5223–5227

Compo GP, Sardeshmukh PD (2009) Oceanic influences on recent continental warming. Clim Dyn 32:333–342

Crook JA, Forster PM, Stuber N (2011) Spatial patterns of modeled climate feedback and contributions to temperature response and polar amplification. J Clim 24:3575–3592

Dommenget D (2009) The ocean's role in continental climate variability and change. J Clim 22:4939–4952

Dommenget D (2012) Comments on the relationship between land-ocean surface temperature contrast and radiative forcing. J Clim 25:3437–3440

Drost F, Karoly D, Braganza K (2012) Communicating global climate change using simple indices: an update. Clim Dyn 39:989–999

Fasullo JT (2010) Robust land-ocean contrasts in energy and water cycle feedbacks. J Clim 23:4677–4693

Forster PM, Blackburn M, Glover R, Shine KP (2000) An examination of climate sensitivity for idealised climate change experiments in an intermediate general circulation model. Clim Dyn 16:833–849

Geoffroy O, Saint-Martin D, Ribes A (2012) Quantifying the sources of spread in climate change experiments. Geophys Res Lett 39:L24703

Geoffroy O, Saint-Martin D, Olivié DJL, Voldoire A, Bellon G, Tytéca S (2013a) Transient climate response in a two-layer energy-balance model. Part I : analytical solution and parameter calibration using CMIP5 AOGCM experiments. J Clim 26:1841–1857

Geoffroy O, Saint-Martin D, Bellon G, Voldoire A, Olivié DJL, Tytéca S (2013b) Transient climate response in a two-layer energy-balance model. Part II : representation of the efficacy of deep-ocean heat uptake and validation for CMIP5 AOGCMs. J Clim 26:1859–1876

Geoffroy O, Saint-Martin D, Voldoire A, Salas-Mélia D, Sénési S (2014a) Adjusted radiative forcing and global radiative feedbacks in CNRM-CM5, a closure of the partial decomposition. Clim Dyn 42:1807–1818

Geoffroy O, Saint-Martin D (2014b) Pattern decomposition of the transient climate response. Tellus A 66:23393

Gregory JM (2000) Vertical heat transports in the ocean and their effect on time-dependent climate change. Clim Dyn 16:505–515

Gregory JM et al (2004) A new method for diagnosing radiative forcing and climate sensitivity. Geophys Res Lett 31:L03205

Gregory JM, Webb MJ (2008) Tropospheric adjustment induces a cloud component in CO_2 forcing. J Clim 21:58–71

Hansen J, Lacis A, Rind D, Russell G, Stone P, Fung I, Ruedy R, Lerner J (1984) Climate sensitivity: analysis of feedback mechanisms. In: Hansen JE, Takahashi T (eds) Climate processes and climate sensitivity, AUG Geophysical Union Monograph 29, Maurice Ewing, vol 5. American Geophysical Union, Washington D.C, pp 130–163

Hansen J, Sato M, Ruedy R (1997) Radiative forcing and climate response. J Geophys Res 102:6831–6864

Hansen J et al (2005) Efficacy of climate forcings. J Geophys Res 110:D18104

Held IM, Soden BJ (2006) Robust responses of the hydrological cycle to global warming. J Clim 19:5686–5699

Held IM, Winton M, Takahashi K, Delworth T, Zeng F, Vallis GK (2010) Probing the fast and slow components of global warming by returning abruptly to preindustrial forcing. J Clim 23:2418–2427

Huntingford C, Cox PM (2000) An analogue model to derive additional climate change scenarios from existing GCM simulations. Clim Dyn 16:575–586

Hwang Y-T, Frierson DMW (2010) Increasing atmospheric poleward energy transport with global warming. Geophys Res Lett 37:L24807

Joshi MM, Gregory JM, Webb MJ, Sexton DMH, Johns TC (2008) Mechanisms for the land/sea warming contrast exhibited by simulations of climate change. Clim Dyn 30:455–465

Joshi MM, Lambert FH, Webb MJ (2013) An explanation for the difference between twentieth and twenty-first century land-sea warming ratio in climate models. Clim Dyn 41:1853–1869

Lambert FH, Chiang JCH (2007) Control of land-ocean temperature contrast by ocean heat uptake. Geophys Res Lett 34:L13704

Lambert FH, Webb MJ, Joshi MM (2011) The relationship between land-ocean surface temperature contrast and radiative forcing. J Clim 24:3239–3256

Manabe S, Stouffer RJ, Spelman MJ, Bryan K (1991) Transient responses of a coupled ocean–atmosphere model to gradual changes of atmospheric CO_2. Part I: annual mean response. J Clim 4:785–818

Manabe S, Spelman MJ, Stouffer RJ (1992) Transient responses of a coupled ocean–atmosphere model to gradual changes of atmospheric CO_2. Part II: seasonal response. J Clim 5:105–126

Rose BEJ, Armour KC, Battisti DS, Feldl N, Koll DDB (2014) The dependence of transient climate sensitivity and radiative feedbacks on the spatial pattern of ocean heat uptake. Geophys Res Lett 41:1071–1078

Sherwood S, Bony S, Boucher O, Bretherton CS, Forster P, Gregory J, Stevens B (2014) Adjustments in the forcing-feedback framework for understanding climate change. Bull Am Meteorol Soc (in press). doi:10.1175/BAMS-D-13-00167.1

Sobel AH, Bretherton CS (2000) Modeling tropical precipitation in a single column. J Clim 13:4378–4392

Sutton RT, Dong BW, Gregory JM (2007) Land-sea warming ratio in response to climate change: IPCC AR4 model results and comparison with observations. Geophys Res Lett 34:L02701

Taylor KE, Stouffer RJ, Meehl GA (2011) An overview of CMIP5 and the experiment design. Am Meteorol Soc Bull. doi:10.1175/BAMS-D-11-00094.1

Vial J, Dufresne J-L, Bony S (2014) On the interpretation of inter-model spread in CMIP5 climate sensitivity estimates. Clim Dyn 41:3339–3362

Voldoire A, Sanchez-Gomez E, Salas y Mélia D, Decharme B, Cassou C, Sénési S, Valcke S, Beau I, Alias A, Chevallier M, Déqué M, Deshayes J, Douville H, Fernandez E, Madec G, Maisonnave E, Moine M-P, Planton S, Saint-Martin D, Szopa S, Tyteca S, Alkama R, Belamari S, Braun A, Coquart L, Chauvin F (2013) The CNRM-CM5.1 global climate model: description and basic evaluation. Clim Dyn 40:2091–2121

Winton M, Takahashi K, Held IM (2010) Importance of ocean heat uptake efficacy to transient climate change. J Clim 23:2333–2344